MSc in Photonics

PHOTONICS**BCN**

Universitat Politècnica de Catalunya (UPC)
Universitat Autònoma de Barcelona (UAB)
Universitat de Barcelona (UB)
Institut de Ciències Fotòniques (ICFO)

http://www.photonicsbcn.eu

Master in Photonics

MASTER THESIS WORK

Development of a fluorescence imaging system for a quantum gas experiment

Julio Sanz Sánchez

Supervised by Dr. Leticia Tarruell, (ICFO)

Presented on date 10th September 2015

Registered at

Escola Tècnica Superior d'Enginyeria de Telecomunicació de Barcelona

Development of a fluorescence imaging system for a quantum gas experiment

Julio Sanz Sánchez

ICFO-Institut de Ciències Fotòniques, Parc Mediterrani de la Tecnologia, 08860 Barcelona, Spain

E-mail: julio.sanz@icfo.es

August 2015

Abstract. In this report we present a technique for imaging the momentum distribution of an ultracold atomic gas in 3D and with single atom resolution. We describe the first experimental steps taken to implement it in a quantum gas experiment and the development of a numerical simulation of the detection process.

Keywords: ultracold quantum gases ,Littrow , fluorescence , single atom resolution, thin light sheet

1. Introduction

Being able to create controllable quantum systems provides a novel tool for studying many condensed-matter phenomena. Nowadays we can generate quantum degenerate gases, expose them to arbitrary potential landscapes using optical lattices [1] and tune the interactions between atoms adjusting external magnetic fields . Thanks to that we are able to prepare a wide variety of quantum systems to perform quantum simulations and get insights into condensed-matter physics.

In order to extract information from the experiments we need to image the atoms. There are two imaging techniques for that: in-situ and Time of Flight (ToF). The former gives information about the real space distribution whereas the latter gives information about the momentum space. Normally, both involve integration along the observation direction, losing information about one dimension. To be able to obtain a 3D information there have been several approaches. For instance, it is possible to make a 3D tomography in real space by letting a cloud of He^* fall into a microchanel plate [2]. Recently, Bücker et al. [3] demonstrated that it is possible to make a 3D tomography in momentum space for ^{87}Rb making fluorescence imaging with the help of a thin light sheet (LS). However, it is not clear if this technique can be used with potassium.

The aim of this master thesis is to study the possibility of applying it in our experiment. In order to introduce the reader into the topic we will describe our experimental setup as well as the generation of a quantum gas in Sec 2. In Sec. 3

we will introduce the basic principles of the fluorescence imaging technique using a thin LS. We subsequently describe the experimental and theoretical work carried out during this master thesis. In Sec. 4 we detail the construction of a laser to be used for atomic physics experiments. In Sec. 5 we present the characterization of an objective designed for diffraction limited resolution. In Sec. 6 we analyse the simulation of cold atoms falling through a thin LS. We conclude our study in Sec. 7 and present the plan for further investigation on the topic in Sec. 8.

2. Experimental setup and Bose Einstein Condensation of ^{41}K

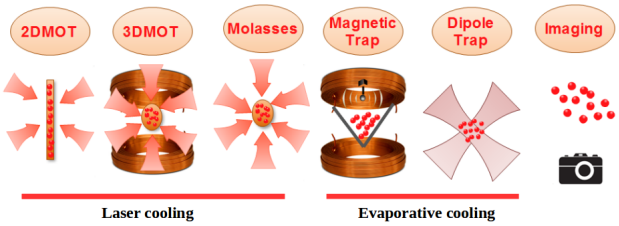

Figure 1. Schematic of the cooling strategy to produce quantum gases.

In the experimental setup that we use in our group we have decided to study quantum gases of potassium. There are two reasons for this choice. On the one hand, we can have a good control of the interactions between its different isotopes thanks to suitable Feshbach resonances. And on the other hand potassium has favourable properties for fluorescence imaging. This allows to have a flexible system with which we will study Bose-Bose, Fermi-Bose and Fermi-Fermi mixtures in the strongly interacting regime. The experimental setup for producing degenerate gases is currently being developed . In fact, during my thesis, we have already been able to generate a BEC of ^{41}K atoms and to make a magneto optical trap (MOT) of ^{40}K atoms for the first time.

The strategy that we use to cool the atoms is sketched on figure 2 and is mainly divided into two parts: laser cooling and evaporative cooling in conservative traps.

- The experiment starts in a chamber with a high vapor pressure of natural potassium. A cold atomic beam is generated from the background pressure using a 2DMOT.
- The atoms are sent from the 2DMOT chamber to an Ultra High Vacuum (UHV) chamber (science chamber) where they are captured in a 3D MOT. In order to increase the density, they are subsequently compressed in a CMOT.
- Gray optical molasses on the D1-line are used to obtain efficient sub-Doppler cooling.
- The atoms are prepared in $|F = 2, m_F = 2 >$ by optical pumping and captured in a magnetic quadrupole trap.
- Radio-frequency (RF) evaporation on the hyperfine transition leads to a phase-space density (PSD $= \mathrm{n}\lambda_T^3$, where n is the atomic density and λ_T is the De Broglie wavelength) of $\sim 10^{-4}$.
- The atoms are transferred to a crossed optical dipole trap and evaporated until we obtain a Bose-Einstein Condensate (BEC) as it is shown in figure 2.

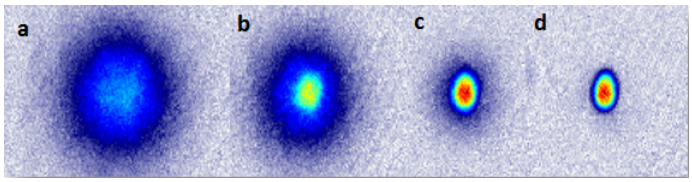

Figure 2. Images taken from absorption imaging in TOF during the evaporative cooling in the dipole trap. a) Thermal cloud T= 120 nK. b) Thermal cloud T=85 nK. c) BEC with thermal fraction at T=40 nK. d) Pure BEC at T= 20 nK.

3. Working principle of the fluorescence imaging with a thin light sheet

The last step after achieving a degenerate quantum gas is to take images to characterize it. The reader should refer to [4] if they want to know more about imaging techniques. In this report we will use the combination of two imaging techniques:

- Time of Flight. An atom cloud is released from a trap and expands during a certain time. Once the cloud is more dilute we take an image of it (usually by absorption imaging). During the expansion every atom can be considered to move without interacting with the others following the laws of Newton. The distance an atom travels during TOF is thus proportional to the initial velocity. Hence, after a certain TOF the images reveal the initial momentum distribution of the cloud.
- Fluorescence imaging. A cloud that is shined with light absorbs and scatters light. The scattering process between atoms and photons can be understood as spontaneous emission. Collecting the light that is scattered from a cloud with an objective is called fluorescence imaging. Notice every time an atom absorbs or scatters a photon it feels a recoil.

Bücker et al. combined both techniques to be able to obtain single atom resolution with ^{87}Rb and make a 3D tomography of the cloud in momentum space using a thin LS. The principle is sketched in figure 3. First, the cloud is released from a trap and expands in TOF. Once it has expanded it crosses a thin LS absorbing and re-emitting photons. Then the emitted photons are collected by an objective below.

This technique has two main advantages. On the one hand, in typical imaging techniques the camera makes an integration over the direction of the imaging beam. With this technique we can make images of every slice by strobing the light or by using a high-speed camera. Thus, it is possible to obtain a 3D tomography. On the other hand, saturation problems are avoided provided that the collection efficiency is just given by a small solid angle. As long as the SNR is enough we can distinguish different atoms if the resolution is smaller than the average inter-particle distance after TOF.

To achieve single atom resolution though we have to study if the photon recoil will distort the image in two different ways. On the one hand, the atom will be moved from its initial position, in average, by an amount σ_c that we will call centroid deviation. And on the other hand, the image will be blurred, in average, by an amount σ_b, that we will call atomic blur. Provided that potassium is twice lighter than rubidium the photon recoil will be higher for potassium. Also we have to be able to achieve a good Signal to Noise Ratio (SNR). Hence, a simulation of the random walk (RW) of the atom on the LS will help us find a trade-off in the optimum parameters to have a good enough SNR

and obtain single atom resolution.

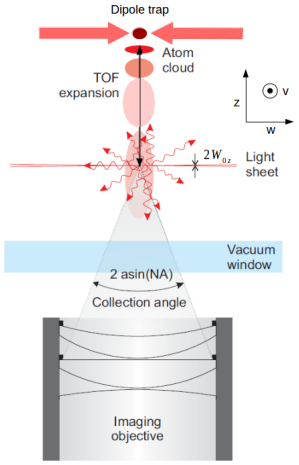

Figure 3. Schematic of the setup for fluorescence imaging with a thin light sheet. The atom cloud is released from the dipole trap and expands during Time of Flight for $TOF = \sqrt{\frac{2z_0}{g}}$, where z_0 is the position of the LS with respect to the center of the science chamber where the atoms are held. The LS has a thickness of $2W_0 << RMS_{cloud}$ so that each slice of the cloud absorbs and reemits photons while it passes through the LS. A fraction of the reemited photons $f_c \approx \frac{NA^2}{4}$ is collected by the objective, that is designed for correcting the aberrations introduced by the vacuum window. In this picture we define the axis that we will use along the report ($\vec{v}\times\vec{w} = \vec{z}$). This image was adapted from one in reference [3].

To be able to develop a system for fluorescence imaging with a thin LS, during this master thesis, I have worked both in the experimental construction and the simulation analysis. The experimental development has consisted on building and characterizing a single mode laser in Littrow configuration (see Sec.4) and improving and characterizing an existing home-made objective with diffraction limited resolution (see Sec.5). The theoretical work has been based on Monte Carlo simulations of the RW of the atoms in the LS using a code I wrote (see Sec.6).

4. Construction of a single mode laser in Littrow configuration

4.1. A Laser for Atomic Physics

Imaging, and in general all laser manipulation of potassium atoms, requires lasers that can resolve the level structure shown in figure 4. The energy shift between the levels is on the order of a few tenths of MHz with a linewidth of 6MHz for the D1 and D2 transitions. Thus, we need lasers whose bandwidth is a few orders of magnitude smaller.

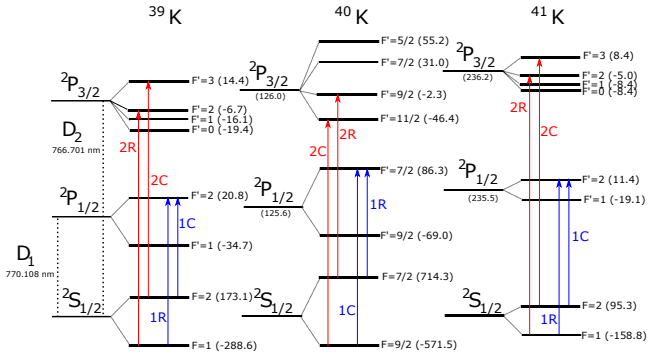

Figure 4. Fine and hyperfine structure of the three isotopes of potassium. In parenthesis we show (in MHz) the energy shifts of the both fine states from ^{40}K and ^{41}K with respect to those of ^{39}K, and also the energy difference between each hyperfine state with respect to the energy of the fine state to which they correspond. We also show the cooling and repumping transitions used. In the experiment, the transitions for the D_2-line will be red detuned and the ones corresponding to the D_1-line will be blue detuned. Frequencies taken from [5].

Among the lasers available at 766.7nm, semiconductor Diode Lasers (DL) are a good choice because they are cheap, easy to manipulate and very efficient. However the small size of a DL makes their linewidth too huge for atomic physics experiments. Therefore to use DL we need to have longer cavities. A possible configuration to solve that problem is called Littrow configuration. The main scheme of this lasers is sketched

in figure 5a . The strategy to enlarge the cavity consists on using a diffractive grating that acts as the mirror of a bigger cavity in such a way that the 1st order of diffraction comes back into the diode for generating feedback. The 0th order gets reflected out.

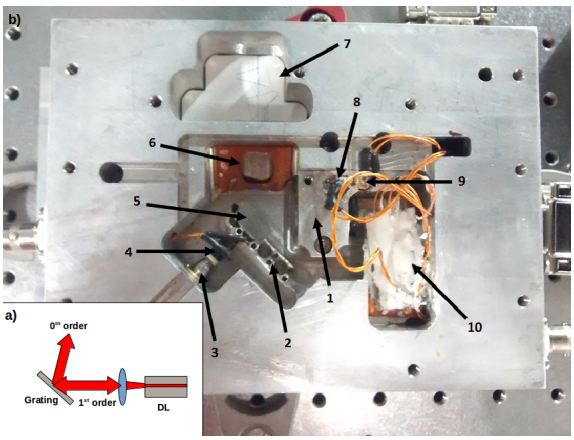

Figure 5. a) Schematic of the Littrow configuration. b) Main piece of the laser. Made from aluminum in the Mechanical Workshop@ICFO 1. Collimator holder. Inside there is a Thorlabs collimator (LT230P-B) in which a diode laser (TOPTICA) is placed. 2. Grating holder. 3. Precision adjustment screw (New Focus, 9376-K). 4. Piezoelectric element (Piezomechanik, PSt150/5/5). 5. UV Diffraction Holographic grating (Thorlabs, GH13-18U). 6. Brewster window. 7. Position of anamorphic prism pair (Thorlabs, PS871-B). 8. Thermocouple (Farnell,). 9.Thermistor (Thorlabs, AD590). 10. Protection circuit, Electronic Workshop@ICFO.

This kind of laser allows to tune the wavelength in three different ways: changing the temperature, the injection current and angle of the grating (provided that the angle of diffraction depends on the wavelength). Hence, fine tuning requires, on the one hand, a fine control of temperature and injection current; and on the other hand a good mechanical stability. For a good control of temperature and current we will make an active stabilization using a PID. To have a good mechanical stability we chose a design based on reference [6] because it seems it can have more stability than previous designs used by members of our team [7]. This is because the main part of the laser is made in just one piece of aluminum as we can see in figure 5b.

4.2. Construction of the laser and characterization

To know the details of the assembly process of the laser the reader should refer to [8]. Hereby we will detail the important steps of the process, characterize the laser, explain the problems that we found while building it.

The important steps followed during the construction of the process were:

- Testing the electronic protection circuit, designed for avoiding high currents flowing through the diode or unwanted current spikes that could damage it.
- Adjust PID-temperature controller gains.
- Collimate the DL beam. $R_p = 76.5\%$ p-polarization over total power at 150 mA.
- Align the DL to obtain feedback. To do so we changed the angle of the grating with an adjustment screw and the angle of the DL with two screws.Once we obtained feedback we optimized the alignment by trying to reduce the lasing threshold iteratively. After the first alignment stage the threshold was found to be $I_{th} = 125mA$ (at 777,5nm) with an output power of 51 mW at I=225mA.
- Tune the laser frequency (using a wavemeter) in a first stage modifying temperature and injection current, and in a second stage, and once we started to be constrained

by mode hopping (Free Spectral Range FSR = 0.05nm), playing with the angle of the grating. A further tuning with the piezoelectric would have been needed, but we realized that after a certain pressure the piezo stops working. Thus we would have to change the piezo to lock the laser with a PID to a potassium transition.

- Charaterize the output beam. The shape was measured to be elliptical with waists $W_p = 255\mu m$, $W_s = 214\mu m$ with $R_p = 51$ % an p-polarization ratio after the Brewster window. The output power vs. injection can be seen in figure 6 (current threshold $I_{th} = 155mA$, slope 0.5mW/mA). Notice though that the increase is not linear indeed. This could be because the DL we are using was damaged.
- Align the optical isolator. Playing with its angle we achieved a maximum transmission of 85% and an output power of P = 21 mW.

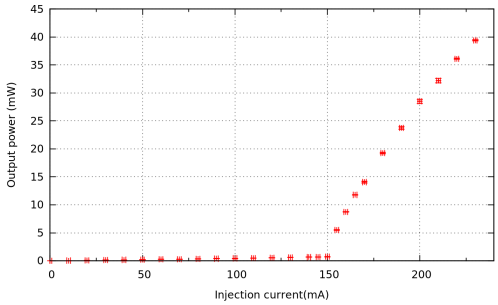

Figure 6. Output power vs. injection current of the laser for $\lambda = 766.7007nm$.

5. Characterizing a home-made objective for diffraction limited resolution

Having a high resolution objective will be really important in our experiment to extract information from real and momentum space. For that an objective had already been designed when I started my master. My work in this thesis has been to assemble a test set-up which mimics the experiment, test the objective, improve the mounting and develop the alignment procedure.

The objective that was designed contains a commercial aspherical lens and a custom-made meniscus for correcting the aberrations introduced by the vacuum window. A doublet lens is used after that to focus the imaging beam onto a camera. The objective design was constrained by the the position of the atoms in the UHV chamber. It was made for making in-situ and TOF imaging, and to work on 767nm as main resolving wavelength with diffraction limited resolution ($NA \approx 0.47$). This led to a design that is supposed to obtain a Field of View $FOV \approx 200\mu m$ and a resolution of $1\mu m$.

To characterize the resolution of a system we measured the Point Spread Function (PSF), which is the response of an imaging system to a point source. In this case a custom-made test target made of gold nanodots deposited onto a glass probe were used as point sources. Fitting the images to a gaussian profile and introducing a corrector factor that we calculated by fitting an Airy disk with a 2D gaussian we can measure the resolution of our system. For measuring the PSF we used spatially incoherent light to avoid unwanted interferences. The setup that we used is sketched in fig. 7a Some images that we took can be seen in figure 5, there we were able to measure a maximum resolution of $\sigma_{res} = 1.5\mu m$ (extracted from fig. 5b).

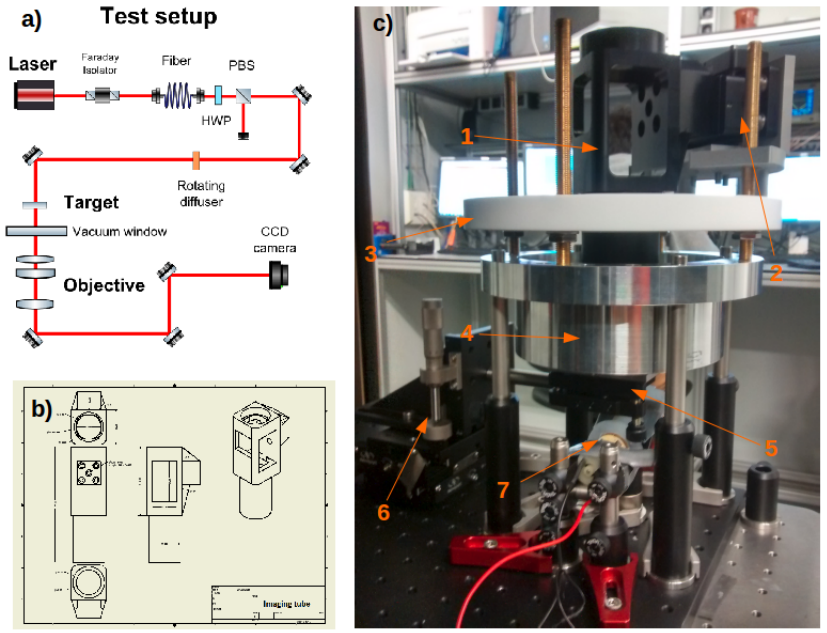

Figure 7. a) Schematic of the test setup. After the laser light is coupled into a fiber it passes through a Half Wave Plate (HWP) and a Polarization Beam Splitter that allow us to change the intensity over the target. Then a rotating diffuser is used to generate spatially incoherent light to avoid interferences. Once the light passes through the target it is collected by an objective and is focused onto a CCD camera. b) Design of the objective mount. c) 1.Objective mount. 2. 5-axis stage for alignment. 3. Water distribution system replica. 4. Vacuum chamber viewport replica. Inside it a vacuum window is placed on the center. 5. 2-axis stage in which the target is placed. 6. 3-axis mount for moving the target. 7. Rotating diffuser.

To improve the resolution of the system we realized during the alignment that there were a few problems that could be improved. On the one hand, the objective mount was held by a 5-axis mount that was placed over it. Given that the 5-axis mount was held by four long bars (see fig. 7c) the mechanical stability was compromised. To solve this problem we designed (CAD design in fig. 7b) a compact mount that was held from the side around 15 cm below as it can be seen in figure 7c. The main advantage is that the 5-axis stage that we use is held over a coil mount, giving more mechanical stability to the system. On the other hand, in the previous design the distance of the objective to the window could not be modified easily, so that with the new design we recovered 1 degree of freedom to align. Nevertheless, the new prototype still could be improved given that the springs of the 5-axis stage are not tight enough for giving mechanical stability to the objective during the alignment process. Further development will be needed to improve it.

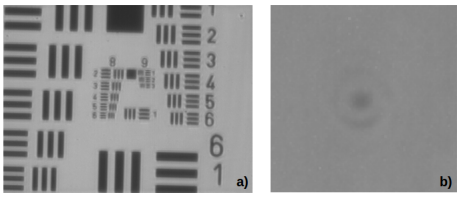

Figure 8. a) Image of USAF 1951 target. The smallest elements in the target have lines of 0.78 μm of width. b) Image of a gold nanodot with a diameter $d \sim 250nm$.

6. Simulating individual atoms falling through a thin light sheet

To understand how the photon - atom scattering will affect the imaging performance we need to make a simulation. For that we will consider that the atoms are described by a two-level system that interacts with the photons with a scattering rate γ_P in equation 1 where γ is the linewidth for ^{41}K, $s_0 = \frac{I}{I_s}$ is the saturation parameter ($I_s = \frac{\pi hc\gamma}{3\lambda^3}$), and

$\Delta = \omega_0 - \omega_L$ is the detuning. For more details see ref.[9].

$$\gamma_P = \frac{\gamma}{2} \frac{s_0 exp(-\frac{2z^2}{W_{0z}^2})}{1 + s_0 exp(-\frac{2z^2}{W_{0z}^2}) + (\frac{2\Delta}{\gamma})^2} \tag{1}$$

The key parameters that will affect the system performance are: the LS waist W_{0z}, the detuning Δ and the saturation parameter s_0. Changing those parameters we will modify the number of emitted photons per atom $< n_{ph/at} >$, the centroid deviation of an atom from its ideal position σ_c and the atom blur σ_b .

To simulate the effect over those parameters a Monte Carlo simulation was made using a program I wrote from scratch based on reference [10]. The basic principle is checking every timestep dt if a pseudo-random generated number is greater or smaller than $e^{-\gamma_P(z,\vec{v})dt}$. In case it is greater we have assumed that the atom absorbs a photon from one of the beams with the same probability, and re-emits it in a random direction with an isotropic probability distribution. After every step the velocities and positions are recalculated using Newton laws. The process is iterated until the atom crosses the LS.

The information we will extract from the simulations is the average Root Mean Square (RMS) displacement in the i-direction $< d_i^2(z) >$ along the falling direction. A second code I developed calculates the information we need for studying the effect of the LS:

- Average number of emitted photons per atom $< n_{ph/at} >= \frac{1}{v_{0z}} \int_{-2W_{0z}}^{2W_{0z}} \gamma_P(z, \vec{v}) dz$
- Centroid deviation $\sigma_c^i = \frac{\frac{1}{v_{0z}} \int_{-2W_{0z}}^{2W_{0z}} \sqrt{<d_i^2(z)>} \gamma_P(z,\vec{v}) dz}{<n_{ph/at}>}$.
- Atomic blur $\sigma_b^i = \sqrt{\frac{\frac{1}{v_{0z}} \int_{-2W_{0z}}^{2W_{0z}} <d_i^2(z)> \gamma_P(z,\vec{v}) dz}{<n_{ph/at}>} - \sigma_c^2}$.

where v_{0z} is the velocity at which the atoms cross the LS.

Another important parameter is the SNR. Provided that in our experiment we will use an Electron Multiplying CCD most of the noise sources can be neglected. Among them Clock-induced charges, dark-counts, spurious background photons and read-out noise can be almost eliminated. Thus we will only consider photon shot noise weighted by a factor 2 ($SNR = \frac{f_c <n_{ph/at}>}{\sqrt{2 f_c <n_{ph/at}>}}$). that appears in the electronic processing of the EMCCD cameras. For more details see reference [10].

6.1. Results and discussion

Following the model that we sketched in the previous section we were able to calculate the atomic blurring (figures 9a-d). From the results we can take several conclusions:

- The simulations confirm that the larger the saturation and the LS waist the larger the blurring.
- The dependence of the blurring on the detuning is really high closer to resonance. Hence, the difference for different waists is smaller for higher red detuning.

- The blurring in the direction of propagation is much higher than on the transverse direction. This is consistent with the fact that the absorption is concentrated on a solid angle of $\frac{2\lambda^2}{\pi W_{0z}^2}$ whereas the fluorescence is spread over the full solid angle, and the fact that we considered the probability to absorb the atoms as equal in both directions. However we expected the opposite result because the Doppler effect should have made molasses over the atoms. For this reason we realized that the Doppler effect was not taken into account properly and that the absorption between the beams should be balanced correspondingly instead of being the same for both beams. For this reason we will consider in the following analysis the transverse blurring as an upper bound provided that the absorption does not play any role on this direction. We will correct this error in future simulations.

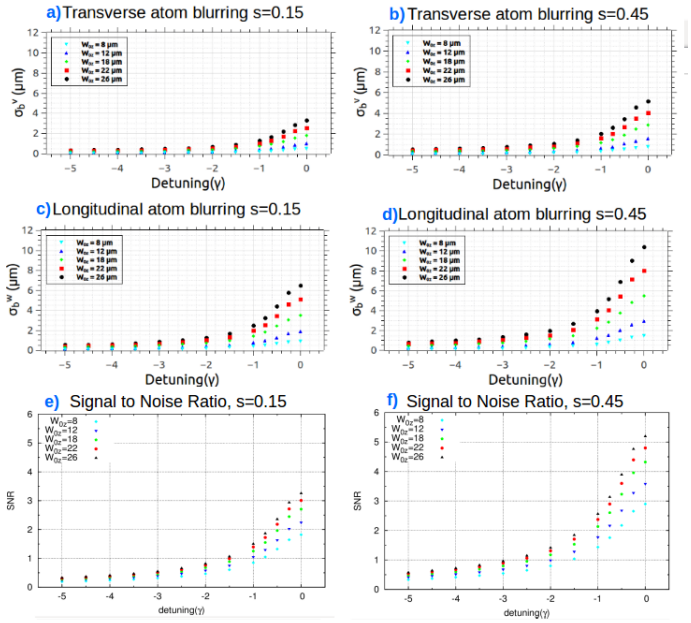

Figure 9. All the images correspond to simulations where N=5000 atoms have been used. The D2 line has been considered in this calculations. a) Longitudinal atom blurring with a saturation parameter of s_0=0.45. b) Transversal atom blurring with a saturation parameter of s_0=0.45. c) Longitudinal atom blurring with a saturation parameter of s_0=0.15. d) Transversal atom blurring with a saturation parameter of s_0=0.15. e) Signal to noise ratio with a saturation parameter of s_0=0.15. f) Signal to noise ratio with a saturation parameter of s_0=0.45.

In figures 9e and 9f we can see the SNR for different values of saturation. As it was expected the SNR is very small for high red detuning provided that only a few photons will be collected by the objective. Hence we need to be close to resonance. Moreover we see that the bigger the saturation parameter the bigger the SNR. An important result is that we see that for beams with $s_0 > 0.4$, $W_{0z} > 22\mu m$ and detuning $\Delta > -\frac{\gamma}{2}$ the SNR is bigger than 4 with which it is possible to work. The bigger SNR that has been calculated up to now in the simulations reaches $SNR \sim 5.2$ at $W_{0z} = 26\mu m$ and $\Delta = 0$. The atomic blur for this values is $\sigma_b = 5\mu m$, so that the resolution of the imaging will be mainly limited by the photon recoil. Moreover we have calculated a centroid deviation of $\sigma_c = 8\mu m$ for this values, which gives a total resolution of 9.4 μm. Thus $\sigma_{tot} = 5,2\mu m$ will limit the minimum average inter-particle distance on the object plane to be able to obtain single atom resolution, whereas 9,4 μm will give a lower bound on the object plane to be able to measure atom-atom correlations.

7. Conclusions

During this project we have been able to: construct and characterize a Littrow laser for an atomic physics experiment with potassium; improve and characterize an objective, and obtain a resolution of $1,5\mu m$; and write a code to simulate the behaviour of cold atoms interacting with a thin light sheet. With this simulation we have been able to: set an upper bound resolution of $5.2\mu m$ to distinguish single atoms; set a lower bound of 9.4 μm to the measurable atom-atom; demonstrate that we can achieve a $SNR > 5$. correlations and discover that the Doppler effect was not implemented effectively in the simulation.

Additionally, I have participated in obtaining the first Bose-Einstein Condensate in Spain , in the optimization of the ^{40}K MOT, and have implemented an application for binning images onto the main experiment controller.

8. Next steps

This work constitutes a feasibility study of light-sheet fluorescence imaging with our apparatus, as well as the first experimental steps towards it. Next steps in the project will be the following. On the experimental side: lock the Littrow laser and integrate it into the main experiment; improve the mounts to increase the stability of the objective and obtain diffraction limited resolution; characterize the EMCCD camera; evaluate the experimental constrains of our experiment: such as suitable TOF, minimum available waist etc.; and design a system for focusing a thin light sheet and implement it. On the theoretical side: we will introduce the Doppler effect in the simulations and we will explore the possibilities with more complex level structures.

Acknowledgments

I want to express my gratitude to Leticia Tarruell for giving me the opportunity to participate in this project and for her good advice. I want to thank Pierrick Cheniney, Luca Tanzi, César Cabrera, Jordi Sastre and Lisa Saemisch for helping everyday and making every day more fun. Special words to my family, Alexandra Belcea and friends, that have cheered me up during the tough moments.

References

[1] Greiner M., Fölling S. 2008 *Nature* **458**, 736-738
[2] Schellekens M. et al. *Science* 2005: **310** (5748), 648-651.
[3] R Bücker et al. 2009 *New J. Phys.* **11** 103039
[4] Ketterle W., Durfee D.S., Samper-Kurn D.M. 1999 *arXiv:cond-mat/9904034*
[5] Tiecke T.G 2010 *Properties of Potassium.* http://staff.science.uva.nl/ tgtiecke/PotassiumProperties.pdf
[6] C. Cook W., Martin P. J., Brown-Heft T. L., Garman J. C., Steck D. A. *Rev Sci Instrum* 2012 **83** (4):043101
[7] Riccia L. et al. *Optics Communications* 1995 **56** 541-549
[8] Steck D. A. *Unibody Laser Assembly*, http://atomoptics-nas.uoregon.edu/unilaser/photos.html
[9] Metcalf H. J. , Straten P. *Laser Cooling and Trapping* 1999, Springer
[10] Bücker R. Master Thesis - *Fluorescence Imaging of Ultracold Atoms* 2007